A Method for Postinjection PET Transmission Measurements with a Rotating Source

Richard E. Carson, Margaret E. Daube-Witherspoon, and Michael V. Green

Department of Nuclear Medicine, National Institutes of Health, Bethesda, Maryland

A method is presented for obtaining accurate positron emission tomography transmission measurements after tracer injection. A transmission scan is performed using a rotating source immediately before or after a conventional emission scan. Sinogram windowing, which removes most scattered and random coincidences, also removes most of the emission counts contaminating the transmission measurement. Data from the emission scan can be used to subtract the remaining emission counts to produce accurate transmission measurements. For studies with moderate to low emission count rates (e.g., fluorodeoxyglucose) there is little increase in noise in the resulting attenuation correction factors. This method was tested in experiments with phantoms and a rotating source simulator and validated against conventional ring transmission measurements. Applications of the technique can significantly shorten the time between transmission and emission studies, and thereby reduce the likelihood of patient motion and increase scanning throughput.

J Nucl Med 29:1558–1567, 1988

Accurate attenuation correction is important in producing quantitative positron emission tomography (PET) images (*1*). For brain studies, reasonable calculated attenuation corrections based on skull outlines can be performed (*2,3*). These methods introduce no additional variability to the final image at the expense of small biases due to inaccurate head position or size, skull thickness, and density. For slices through the lower head and neck or whole-body studies, some form of transmission measurement is essential.

Theoretically, biases in emission images are avoided by direct measurement of the distribution of attenuation. However, unbiased transmission measurements require accurate scatter correction (*4*). Unfortunately, transmission measurements also add noise to the emission data. This effect can be minimized by appropriate smoothing (*5*) or by using the transmission scan to define regions of uniform attenuation (*6*). Conventionally, transmission measurements are performed before tracer administration. For studies that require a long uptake period, there is significant time between transmission and emission scans, e.g., at least 45 min for conventional fluorodeoxyglucose (FDG) studies. This long period of scanner time limits throughput and increases the likelihood of patient motion. Significant movement produces glaring artifacts, while subtle motions produce small, less easily detected, biases.

Ideally, the transmission measurement would be made concurrent with the emission scan. SPECT offers the possibility for such simultaneous measurements through the use of two energy windows (*7*). For PET, the transmission measurement can be done immediately following or preceding the emission scan. The emission counts contaminating the transmission measurement are then subtracted to produce accurate attenuation correction factors. One difficulty is that even for fairly low count studies, the emission count rate along a central projection line is a significant fraction of that from the transmission ring, resulting in a large increase in noise. Errors in subtraction of the emission data due to biologic clearance or accumulation of tracer between the two scans will also be propagated into the final emission image.

Recently, a new method for performing transmission measurements with a rotating rod or pin source has been proposed (*8*) and applied (*9*). The scanner monitors the source position as it rotates about the patient aperture and rejects coincidences that do not intersect the source position. This process, called sinogram windowing, removes most scattered and random coincidences from the transmission measurement, thus removing bias and reducing noise.

We propose the use of a rotating source for transmis-

Received Sept. 8, 1987; revision accepted Mar. 28, 1988.

For reprints contact: Richard E. Carson, PhD, Dept. of Nuclear Medicine, National Institutes of Health, Building 10, Room 1C-401, Bethesda, MD 20892.

sion measurements after tracer injection. This approach increases scanner throughput and reduces potential subject movement between transmission and emission scans with minimal effects on the accuracy and noise of the attenuation measurements. The sinogram windowing performed by the electronics eliminates most of the emission counts as well as randoms and scatter. The remaining emission counts are removed by subtracting data obtained from the emission scan. Since the radioactivity concentration in the pin source is much higher than in the transmission ring, the emission counts are a much smaller fraction of the total counts, so that emission subtraction generates only a small increase in error.

The purpose of this paper is to present this method and validate it against conventional ring transmission measurements. Combined transmission/emission studies were performed using both a ring source and a rotating source simulator. Preliminary results of this study have been previously reported (*10*).

METHODS

Postinjection Transmission Measurements

The following is a derivation of the equations for subtraction of emission contamination from a combined transmission/emission (T+E) study using either a ring or rotating source. Definitions are listed in Table 1. All radioactivity values are corrected for decay to a common time and reflect count rates along a single projection line.

During a transmission scan performed before injection of the patient using a ring or rotating source, the measured count rate along a single projection line C_t, is

$$C_t = a_p I + S_t + R_t \quad (1)$$

TABLE 1
Definitions

a_p	Attenuation factor due to the patient.
a_s	Attenuation factor due to transmission source.
C_e	Measured count rate in emission scan.
C_t	Measured count rate in transmission scan.
$C_{(t+e)}$	Measured count rate in T+E scan.
E	Unattenuated true coincidence rate of emission source.
f	Fraction of time that projection counting is enabled.
I	Unattenuated true coincidence rate of transmission source.
R_e	Random rate in emission scan.
R_t	Random rate in transmission scan.
$R_{(t+e)}$	Random rate in T+E scan.
S_e	Scatter rate in emission scan.
S_t	Scatter rate in transmission scan.
$S_{(t+e)}$	Scatter rate in T+E scan.

where I is the unattenuated true coincidence rate of the transmission source, a_p is the attenuation factor due to the patient, and S_t and R_t are the rates of scattered and random coincidences. The true count rate I will be comparable for ring and rotating source configurations if there is equal total radioactivity in each. For the rotating source, coincidences will be collected along this projection line only when it is intersected by the rotating source. Therefore, the rate of scattered or random coincidences will be much lower than in a conventional ring study.

For a conventional emission scan, the count rate along a single projection line is

$$C_e = a_p E + S_e + R_e \quad (2)$$

where E is the unattenuated true coincidence rate.

A combined transmission/emission (T+E) study is performed immediately before or after the emission scan, and the data is acquired in an identical manner to the conventional transmission scan. For the rotating source, sinogram windowing is employed during the T+E scan. Assuming no biological clearance or accumulation of tracer between the emission scan and the T+E study, the measured coincidence rate in the combined study, is

$$C_{(t+e)} = a_p I + a_p a_s f E + S_{(t+e)} + R_{(t+e)} \quad (3)$$

The term a_s, the attenuation factor due to the transmission source, is included because the source attenuates the emission signal during the T+E scan. The term f represents the fraction of the total scan time that counting is enabled along this projection line. For the rotating source, f equals the fraction of time that the source intersects this projection line and therefore depends upon the size of the source. For ring sources, f = 1. The scatter rate of the T+E scan is

$$S_{(t+e)} = S_t + a_s f S_e + (\text{additional scatter}) \quad (4)$$

where the (additional scatter) is produced from patient counts that are scattered by the transmission source. The randoms rate in the T+E scan can be expressed as

$$R_{(t+e)} = R_t + a_s f R_e + (\text{additional randoms}) \quad (5)$$

Here the three terms respectively correspond to random coincidences produced by two singles from the transmission source, two singles from the emission source, and one single from each source. Combining Eqs. (2–5) and ignoring the additional scatter and randoms yields an estimate for the transmission count rate

$$\hat{C}_t = C_{(t+e)} - a_s f C_e \quad (6)$$

For a ring source (f = 1), the subtraction of the emission counts can produce a substantial increase in noise in the estimate $\hat{C}_t$. Also, small errors in C_e as a result of biologic clearance or accumulation between the emission study and the T+E scan will produce significant

biases in $\hat{C}_t$. For the rotating source, $f \ll 1$, therefore the noise and bias effects will be much smaller.

Study 1: Ring Phantom Study

A 20-cm cylindrical phantom (18 cm length) containing three internal 4-cm cylinders (air, lucite, and aluminum) was scanned. All studies were performed on the Scanditronix PC1024-7B head scanner (*11*). This tomograph has four rings (seven slices) of paired BGO/GSO crystals with transverse spatial resolution of 5.0 mm and axial resolution of 8–12 mm.

Study procedure. A blank ring scan (4 mCi, 10 min, ^{68}Ga) was obtained. A conventional transmission ring scan (10 min) was performed on the cold phantom. 0.8 mCi of ^{68}Ga was added to the background region, and a T+E scan (12.5 min, to compensate for decay) was performed. Finally, a conventional emission scan (25 min) was performed.

Data processing of ring phantom study. Sinograms were generated for all scans with randoms and deadtime corrections. The emission sinogram was scaled for decay and scan length to be comparable to the T+E sinogram, and transmission data corrected for emission contamination ($\hat{C}_t$) were obtained using equation 6. The transmission scatter correction (*12*) was applied and transmission reconstruction performed. In addition, transmission data were derived from the T+E study without emission subtraction to determine the magnitude of the resulting errors. The emission data were then reconstructed with attenuation corrections derived from the conventional transmission study, processed T+E study (with emission subtraction), and the unprocessed T+E study (without emission subtraction).

Study 2: Ring Patient Study

Study procedure. A blank ring scan (5 mCi, 10 min) was performed, followed by transmission ring scan (5 min) of the patient. The patient was injected with 5 mCi of FDG and after a 45-min uptake period, two spatially interleaved emission scans were performed (10 min each). After the second emission scan, a T+E scan was collected (5 min, 5 mCi in the ring) at the level of the second emission scan, followed by a blank ring scan (10 min).

Data processing followed the same procedure as the ring phantom study.

Study 3: Pin Transmission Study

A device was constructed to simulate the functioning of a rotating source (Fig. 1). It is firmly mounted in the patient port of the Scanditronix PC1024-7B scanner. The arm extending out from the base plate holds a rectangular line source called the "pin" (1 × 2 × 15 cm) at the edge of the patient opening (30 cm diameter). By sequentially moving the control pin into each hole in the base plate, the source is reproducibly placed at 60 positions around the ring. An individual blank or transmission scan is performed with the source at each position and a complete scan can be created by summing the 60 sinograms. The size and positions of the source were designed to ensure that counts are collected along all projection lines.

Study procedure. Two cold uniform attenuating phantoms, 4 and 7 cm in diameter, resting side by side on a 1.6-cm thick lucite holder were studied. Sixty blank pin scans (20 sec each, 3.7 mCi ^{68}Ga in the pin at mid-scan) were collected, followed by sixty transmission pin scans (20 sec each, 2.4 mCi). A conventional blank ring scan (20 min, 3.3 mCi in the ring) was collected, followed by a conventional transmission ring scan (20 min, 2.2 mCi at mid-scan). The total scanning time of the pin scans (60 × 20 sec) was equal to that of the conventional blank or transmission scans (20 min).

Processing of pin transmission study. Sinograms were generated for each blank and transmission pin scan with deadtime correction. Each blank sinogram was scaled for decay to its matching transmission scan. Each pair of blank/transmission sinograms was windowed based on the known position of the source. The window width was 2 cm and all projection counts outside this window were rejected. The blank sinograms were summed, the transmission sinograms were summed, attenuation factors were calculated from the ratio of the sums, and transmission reconstruction was performed. No corrections

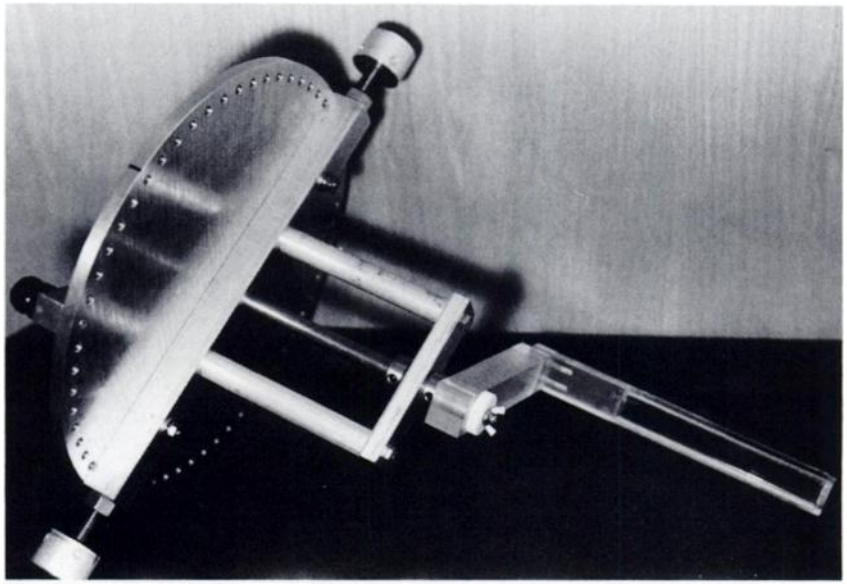

FIGURE 1
Rotating pin source simulator. See text for details.

for random or scattered coincidences were made to the pin data. Conventional reconstruction with randoms and scatter corrections was applied to the ring transmission scan.

Study 4. Pin T+E study

A 20-cm phantom (18 cm length) with three internal 5-cm regions (air, lucite, and water) was studied. There was a 2:1 radioactivity concentration ratio between the internal water region and the background. The total radioactivity in the phantom produced an emission count rate that was 50% higher than average FDG brain studies (6,000 compared to 4,000 cps/slice).

Study procedure. Sixty pin blank scans were acquired (20 sec each, 4.1 mCi ^{68}Ga in the pin at mid-scan), followed by 60 pin T+E scans (20 sec each, 1.6 mCi at mid-scan), and a conventional emission scan (10 min). After the phantom had decayed overnight, a conventional transmission ring study (20 min, 3.7 mCi in the ring) and a blank ring study (20 min, 3.0 mCi) were acquired.

The data processing of the pin T+E study followed the same procedure as that of the pin transmission study with the inclusion of emission subtraction [Eq. (6)]. For each position of the pin, a calculated attenuation was applied to the emission sinogram (to account for the presence of the pin) which was then subtracted from the appropriate transmission sinogram after correction for decay and scan length. No corrections for randoms or scatter were applied to the emission sinogram before subtraction.

RESULTS

Ring Phantom Study

Figure 2 depicts the results from one slice of the ring phantom study. The transmission image from the processed T+E study (B) showed an excellent match to the conventional ring transmission image (A). Results from

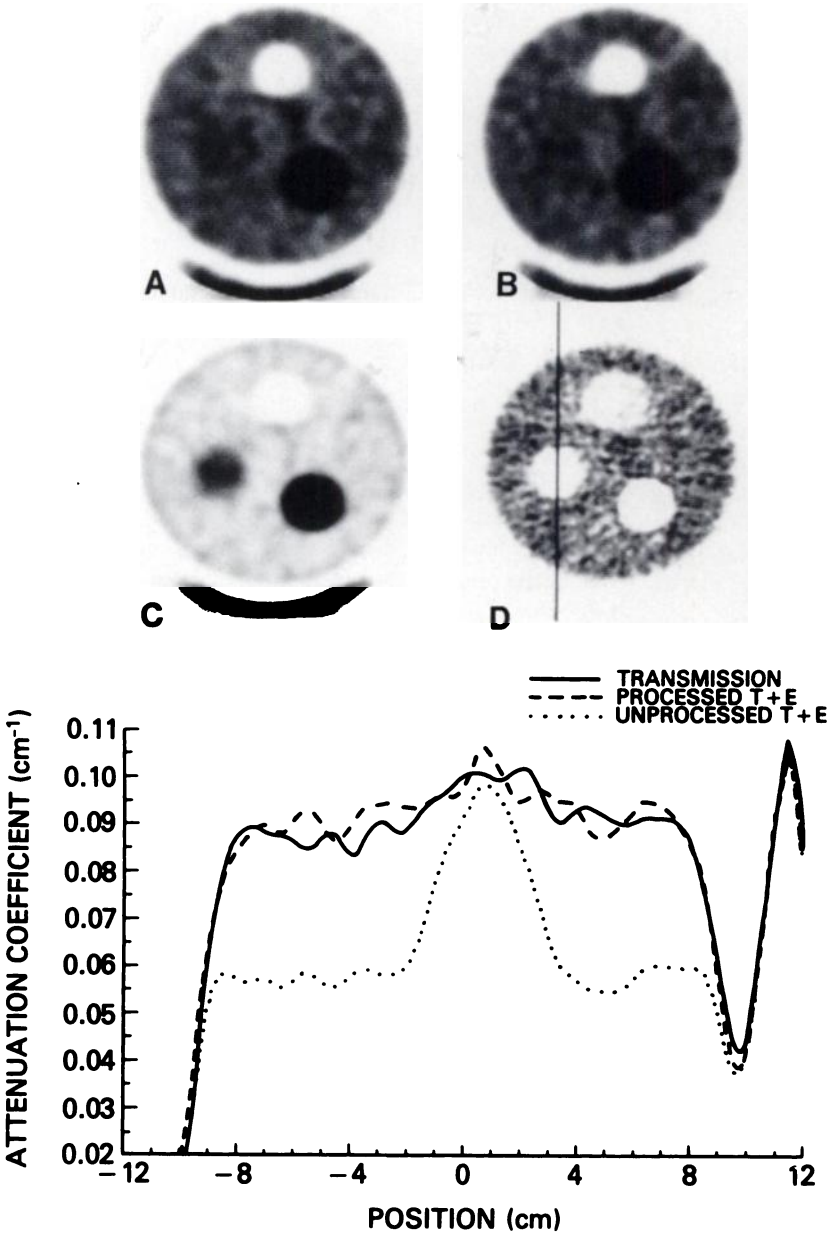

FIGURE 2
Top: Comparison of transmission images from ring phantom study. The phantom contains three 4-cm regions: air (top), lucite (left), aluminum (lower right). A: Conventional transmission image. B: Transmission image produced from processed T+E scan. C: Transmission image produced from T+E scan without emission subtraction. D: Emission image. Bottom: Histogram through transmission images taken at line through lucite cylinder denoted on image D.

region of interest (ROI) analysis of seven slices showed percent differences (B-A) of −0.2 ± 3.0% for the background (nine 2-cm diameter regions were examined) and −0.5 ± 0.4% for the entire image. Without emission subtraction (image C), there was a significant underestimation of attenuation data. ROI percent differences (C-A) were −36 ± 2% and −24 ± 0.5% in background and whole slice, respectively. As seen in the histogram, underestimation of attenuation density was significantly less in regions with no radioactivity, e.g. in the lucite cylinder −9.5 ± 1.9%. There was a 22% increase in pixel-to-pixel standard deviation in the background ROIs of the processed T+E image compared to the ring data, due to the extra emission counts in the T+E scan and the additional noise introduced by emission subtraction.

ROI analysis of emission images showed excellent agreement between attenuation correction obtained from conventional ring data and processed T+E data (−0.5 ± 4.2% and −0.3 ± 0.4% for background regions and whole images). There were significant underestimations using the unprocessed T+E data (−39 ± 6% for background, −20 ± 0.8% for whole slice). There was a 6–7% increase in emission standard deviation using the processed T+E attenuation data in comparison to using the ring data.

Ring Patient Study

Results from the ring patient study are shown in Figure 3. The agreement between conventional transmission data and processed T+E data was poorer. Region-of-interest analysis (8 3-cm diameter regions on seven slices) showed 5.9 ± 3.2% underestimation of attenuation intensity in B with respect to A. This error can be attributed to the difference in time between the emission and T+E scans and the accumulation of FDG during that period (see Discussion). When this incorrect attenuation data is used in the emission reconstruction, it results in a 7.8 ± 3.3% underestimation. Without emission subtraction (image C), the attenuation underestimations are significantly larger (23.5 ± 4.1%) as are the emission underestimations (27.4 ± 11%). In image C and in the histogram data, the pattern of the emission data can be seen in the resulting image, i.e. regions with higher emission activity (gray matter) show larger underestimations than regions with little or no radioactivity (white matter, skull).

Pin Transmission Study

Figure 4 compares transmission images produced from a conventional ring study (A) and the pin study (B). Region of interest analysis (one region on each cylinder occupying ~60% of the area) of images A and B showed percent differences (B-A) of −0.6% and −2.6% for the left and right cylinders, respectively.

Pin T+E Study

Figure 5 summarizes the results of the pin T+E study. Region of interest analysis of the transmission images showed percent differences (B-A) of +1.0 ± 2.7% for the background (6 3-cm diameter regions were examined), −1.1% for the hot cylinder, +0.7% in lucite, and +0.8% for the entire image. Without emission subtraction, ROI percent differences (C-A) were −8.8 ± 1.5%, −17.0%, −1.5%, and −8.2% in background, hot region, lucite, and whole slice, respectively. The magnitude of underestimation of attenuation density was directly related to the regional radioactivity concentration.

ROI comparison of emission images reconstructed with ring attenuation correction versus processed T+E data showed small differences: +0.9 ± 3.6%, −1.04%, and 0.5% for background, hot region, and whole image, respectively. Without emission subtraction from the T+E scan, the emission data were underestimated: −12.4 ± 2.8%, −38.7%, −10.1% for the same regions.

There was a 53% increase in pixel-to-pixel standard deviation in the background ROIs of the processed T+E image compared to the ring data. This is due to the significant difference in activity between the pin and the ring source in the transmission studies (1.6 and 3.7 mCi, respectively). For emission ROIs, there was only a 10% increase in standard deviation (routine transmission smoothing was performed).

DISCUSSION

Ring Studies

The T+E studies using the ring source demonstrate the feasibility of performing postinjection PET transmission measurements. This approach is not ideal because of increased noise in transmission measurements due to the presence and subsequent subtraction of extra emission counts. Quantitative transmission measurements in this case require a very accurate subtraction of the emission contamination. The phantom study produced an excellent match (small bias) between conventional and processed T+E data. The only source of change in emission counts between the T+E scan and the emission scan is radioactive decay, which can be corrected exactly. However, there was still a significant increase in variability in the resulting attenuation data. This noise enhancement would have been even larger if the emission count rate in the phantom had been higher or if a shorter acquisition time had been used to collect the emission data for subtraction.

The patient ring study provided a more realistic evaluation of a ring source for T+E studies. Here, a significant bias was produced which can be attributed to the time difference between the emission scan (55–65 min postinjection) and the T+E scan (68–73 min postinjection). During this time, there is approximately a 5% increase in brain radioactivity predicted from the

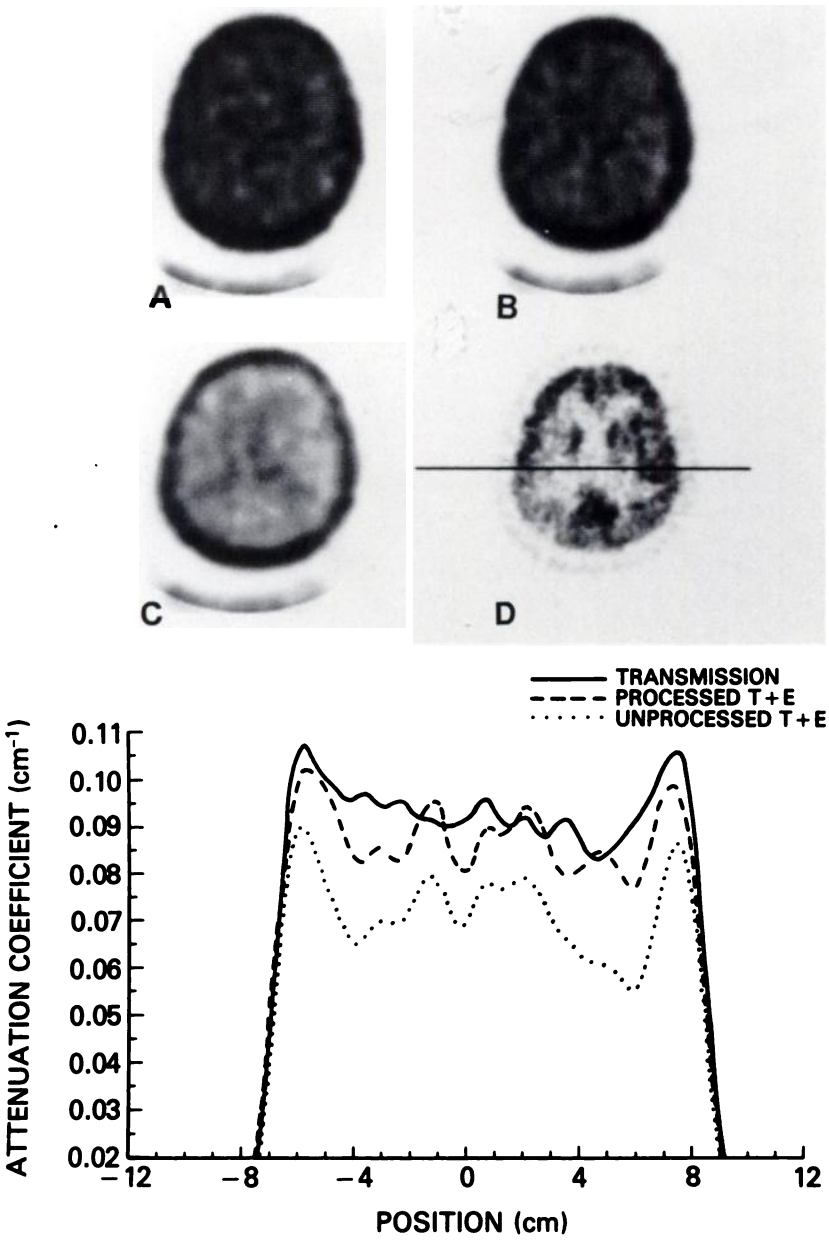

FIGURE 3
Top: Comparison of transmission images from ring patient study. A: Conventional transmission image. B: Transmission image produced from processed T+E scan. C: Transmission image produced from T+E scan without emission subtraction. D: Emission image. Bottom: Histogram through transmission images taken at line denoted on image D.

patient's plasma activity and the FDG model (*13*). This resulted in incomplete subtraction of the emission data from the T+E scan [Eq. (6)]. For the ring source, the emission data was a significant fraction of the T+E data (40–50% for central projection lines). This produced most of the underestimation in the final attenuation data. Using a pin source, the emission counts will be a much smaller fraction of the T+E data ($f \ll 1$, ~0.08 for the pin source simulator), so resulting biases will be much smaller.

Pin Studies

The purpose of the pin transmission study was to compare ring transmission measurements to those obtained from the rotating source. The rotating source simulator is not practical for clinical applications, but instead allows for careful analysis of the characteristics of a rotating source. Unlike a continuously rotating source, independent data acquisitions are performed in each of 60 positions. In this manner, the magnitude of random and scattered coincidences can be directly assessed. Software can perform the function of sinogram windowing which would be performed by the electronics hardware for routine operation.

There were small differences between the ring and pin transmission measurements. One contributing factor to this difference is the scatter correction used in the ring study. The scatter correction algorithm (*12*)

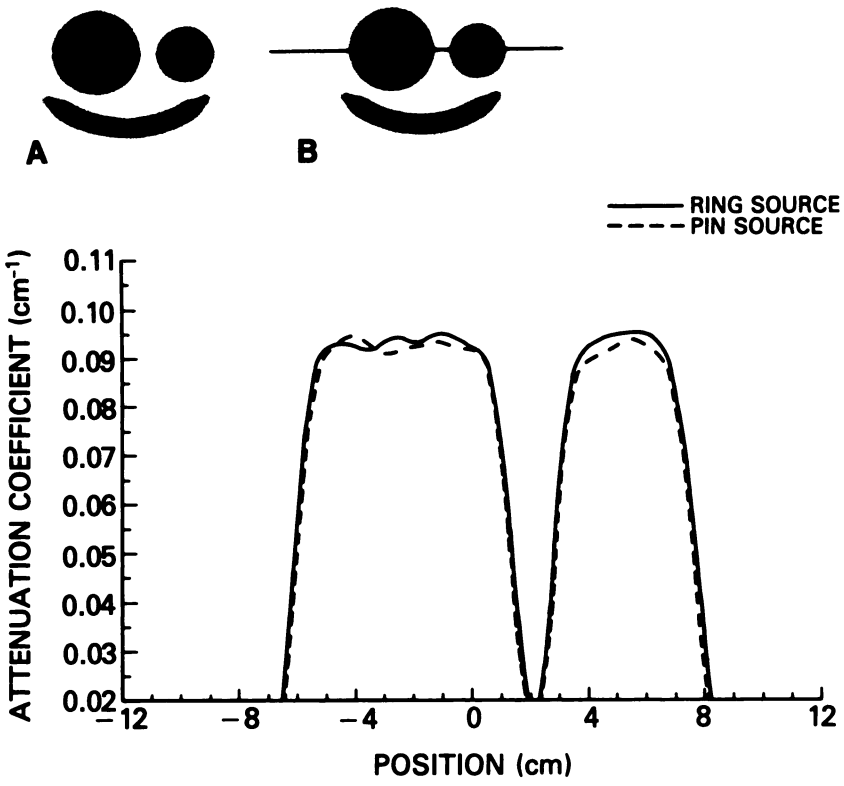

FIGURE 4
Top: Comparison of transmission images from pin transmission study. A: Conventional transmission image. B: Transmission image derived from the 120 pin scans following the procedure described in methods section. Bottom: Histograms through transmission images taken at line denoted on image B.

for the transmission scan requires specification of the size and location of the attenuating object as an ellipse. Since the phantom configuration in this study was not elliptical, small errors were incurred. For the pin study, no scatter correction is applied since most scattered and random coincidences are rejected by the sinogram windowing.

The pin T+E study demonstrates the feasibility of performing accurate postinjection transmission measurements with PET. The contaminating emission counts in the T+E scan can be accurately removed. Small differences in the results can be attributed to differences in the accuracy of the scatter correction for the ring data. Furthermore, by concentrating all the activity in a small source, the ratio of emission to transmission counts is dramatically reduced, so there is very little increase in variability in the transmission measurement. In this study, the highest ratio of emission to transmission pin counts in any projection bin was 15%, and this study was designed as a "worst case" scenario. The pin activity (1.6 mCi during the T+E scan) was significantly less than a 5 mCi source that would be used routinely. The phantom was 50% hotter than typical FDG brain studies. Therefore, in routine use, the emission counts should produce no more than 5% of the T+E counts (less for a smaller pin source). For brain FDG studies, even a 20% error in the emission count rate correction (due to tracer accumulation or clearance) would have only a 1% effect on the final attenuation data.

Applications of the Method

The PET scanning protocols that can most benefit from this method have a significant amount of time between injection and scanning and a moderate to low emission count rate. In these cases, a T+E scan be performed close in time to the standard emission scan. One such tracer method is the single scan approach for measurement of local cerebral metabolic rate of glucose (*13–15*). For example, if an FDG protocol involved two interleaved multi-slice scans, the timing with conventional transmission scans might follow protocol I in Table 2. With the postinjection transmission method, this protocol could be replaced with protocol II. In this case, the time on the scanner bed is reduced from at least 70 min to 30 min. In addition, if it is acceptable to have the subject in another room for the tracer uptake period, the scanner would be available for other studies. In protocol II, there will still be some change in the tracer concentration between the transmission and emission scans, producing some error in the emission subtraction [Eq. (6)]. This error can be reduced by using an appropriate mathematical model to predict the time course of tracer concentration. Alternatively, the effects of physiological accumulation (or clearance) can be reduced by performing two T+E scans at each level, one before and one after the emission scan, as in protocol III of Table 2. Here the mean measurement times of the emission and T+E scans are identical. If tracer concentration is changing linearly during this period, the emission subtraction will introduce no bias.

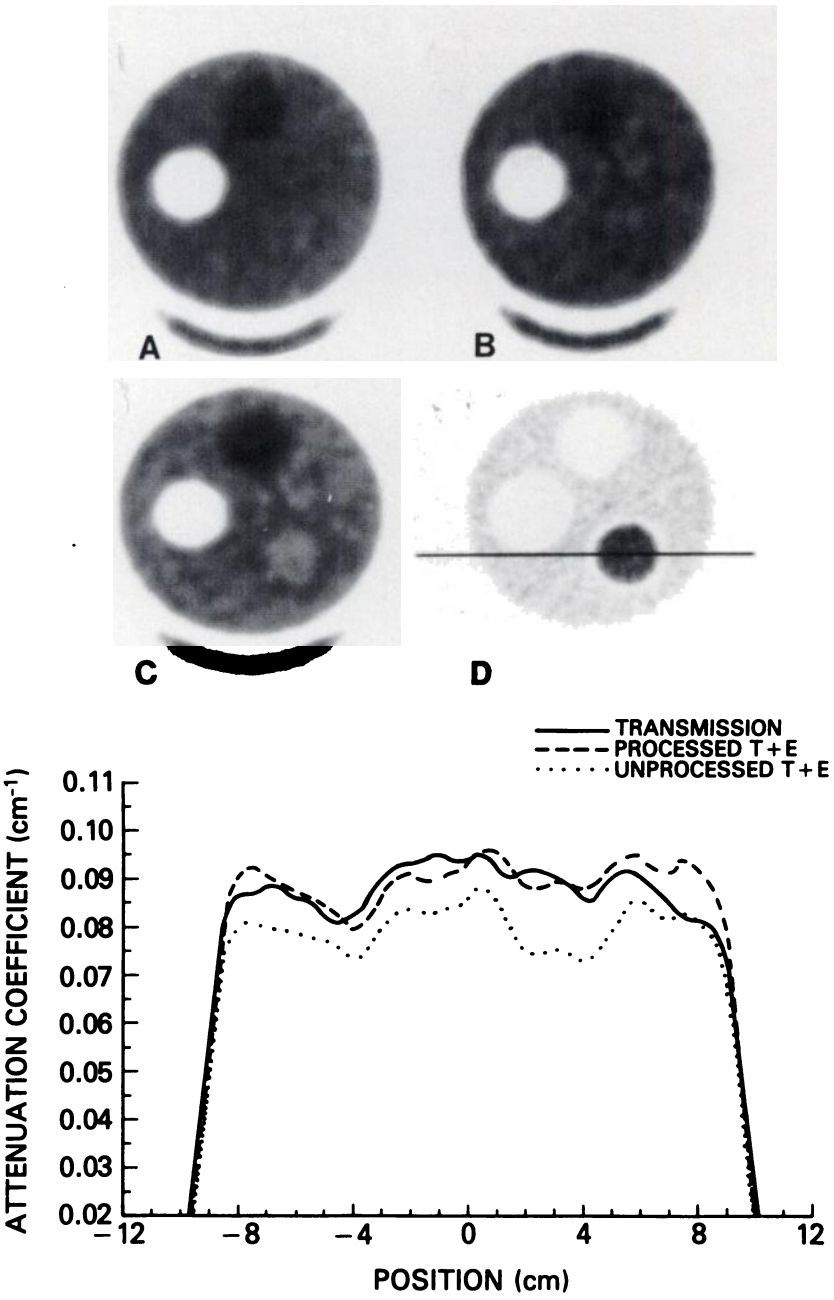

FIGURE 5
Top: Comparison of transmission images from pin T+E study. The phantom contained three 5-cm regions: lucite (top), air (left), and water with twice the background's radioactivity concentration (lower right). A: Conventional transmission image. B: Transmission image produced from processed T+E scan. C: Transmission image produced from T+E scan without emission subtraction. D: Emission image. Bottom: Histogram through transmission images taken at line denoted on image D.

This dual T+E scan approach would only be necessary for studies with higher emission count rates which change significantly during the scanning period.

PET acquisitions often involve multiple scans of the same slice set over time for the purpose of generating tissue time-activity curves for kinetic parameter estimation. One difficulty with the analysis of these studies is subject motion. In order to correct for motion, T+E scans could be performed at regular intervals throughout the scanning sequence. If no motion is detected, all the transmission measurements could be averaged to reduce statistical noise.

One method for improving our postinjection transmission method may be to combine it with the boundary method for attenuation correction (*6*). The latter method uses edge-finding techniques to determine regions of uniform attenuation from short, noisy transmission scans. A combination of these methods offers low noise in the attenuation correction factors, short transmission scans, and the minimum time between emission and transmission scans.

Limitations of the Method

A number of issues require additional study to determine the limitations of this method. As defined in Eqs. (4) and (5), there are additional scattered and random coincidences collected in the T+E scan due to the interaction of the emission object and the transmission

TABLE 2
Sample Protocols

Protocol I. Pre-injection transmission scans

Min postinjection	Study
−10:−5	Transmission I
−5:0	Transmission II
0	FDG injection
40:50	Emission I
50:60	Emission II

Protocol II. Single postinjection transmission scan

Min postinjection	Study
35:40	T+E I
40:50	Emission I
50:60	Emission II
60:65	T+E II

Protocol III. Dual postinjection transmission scans

Min postinjection	Study
37.5:40	T+E Ia
40:50	Emission I
50:52.5	T+E Ib
52.5:55	T+E IIa
55:65	Emission II
65:67.5	T+E IIb

source. Because of the use of sinogram windowing, however, the amount of both scattered and random coincidences in this measurement will be small. In fact, the magnitude of these effects will be much more significant with ring sources (*4*) where appropriate scatter corrections are particularly important (*12,16*).

An additional limitation of the method is the noise propagation of the emission subtraction [Eq. (6)]. The magnitude of this effect will depend on the relative numbers of the emission and transmission events. In addition, the error propagation characteristics will be different if the emission activity is uniformly distributed or localized in small regions (e.g., heart).

The noise level of the final attenuation correction factors will depend on the length of the T+E study, the activity of the transmission source, as well as the emission subtraction. Since it is desirable to have the shortest possible transmission scans, the activity in the source should be as high as possible so long as accurate dead-time corrections can be made. For T+E studies, a somewhat lower source strength would be appropriate to allow for the presence of emission counts. Note, however, that the use of a rotating source has already improved the statistical quality of the data compared to ring transmission sources of the same strength by direct removal of most random and scattered coincidences (*8*).

CONCLUSION

We conclude that for appropriate tracer methods, quantitative transmission measurements can be accomplished with postinjection transmission scans using a rotating source. This approach will reduce the total time that subjects must remain on the scanner bed and provide increased accuracy by minimizing the time for possible patient motion.

ACKNOWLEDGMENTS

The authors wish to thank Drs. Stephen Bacharach and Peter Herscovitch for valuable discussions and helpful advice, and Paul Baldwin for technical assistance.

REFERENCES

1. Huang SC, Hoffman EJ, Phelps ME, et al. Quantitation in positron emission computed tomography: 2. Effects of inaccurate attenuation correction. *J Comput Assist Tomogr* 1979; 3:804–814.
2. Bergstrom M, Litton J, Eriksson L, et al. Determination of object contour from projections for attenuation correction in cranial positron emission tomography. *J Comput Assist Tomogr* 1982; 6:365–372.
3. Tomitami T. An edge detection algorithm for attenuation correction in emission CT. *IEEE Trans Nucl Sci* 1987; NS-34:309–312.
4. Chan B, Bergstrom M, Palmer MR, et al. Scatter distribution in transmission measurements with positron emission tomography. *J Comput Assist Tomogr* 1986; 10:296–301.
5. Palmer MR, Rogers JG, Bergstrom M, et al. Transmission profile filtering for positron emission tomography. *IEEE Trans Nucl Sci* 1986; NS-33:478–481.
6. Huang SC, Carson RE, Phelps ME, et al. A boundary method for attenuation correction in positron emission computed tomography. *J Nucl Med* 1981; 22:627–637.
7. Bailey DL, Hutton BF, Walker PJ. Improved SPECT using simultaneous emission and transmission tomography. *J Nucl Med* 1987; 28:844–851.
8. Carroll LR, Kretz P, Orcutt G. The orbiting rod source: Improving performance in PET transmission correction scans. In *Emission computed tomography: current trends.* New York: Society of Nuclear Medicine, 1983: 235–247.
9. Thompson CJ, Dagher A, Lunney DN, et al. A technique to reject scattered radiation in PET transmission scans. In: Nalcioglu O, Cho ZH, Budinger TF, eds. *International workshop on physics and engineering of computerized multidimensional imaging and processing.* Proc. SPIE, 1986; 617:244–253.
10. Carson RE, Daube-Witherspoon ME, Green MV. A method for post-injection PET transmission measurements with a rotating pin source. *J Nucl Med* 1987; 28:1073–1074.
11. Daube-Witherspoon ME, Holte S, Green MV. Performance of Scanditronix PC1024-7B PET scanner. *J Nucl Med* 1987; 28:607–608.
12. Bergstrom M, Eriksson L, Bohm C, et al. Corrections for scattered radiation in a ring detector positron camera by integral transformation of the projections. *J Comput Assist Tomogr* 1983; 7:42–50.
13. Huang SC, Phelps ME, Hoffman EJ, et al. Noninvasive determination of local cerebral metabolic rate of glucose in man. *Am J Physiol* 1980; 238:E69–E82.
14. Reivich M, Kuhl D, Wolf A, et al. The ^{18}F-fluoro-

deoxyglucose method for the measurement of local cerebral glucose utilization in man. *Circ Res* 1979; 44:127–137.
15. Phelps ME, Huang SC, Hoffman EJ, et al. Tomographic measurement of local cerebral glucose metabolic rate in humans with (F-18)2-fluoro-2-deoxy-D-glucose: validation of method. *Ann Neurol* 1979; 6:371–388.
16. Bendriem B, Soussaline F, Campagnolo R, et al. A technique for the correction of scattered radiation in a PET system using time-of-flight information. *J Comput Assist Tomogr* 1986; 10:287–295.